American Mineralogist, Volume 80, pages 833–840, 1995

An Fe analogue of kinoshitalite from the Broken Hill massive sulfide deposit in the Namaqualand Metamorphic Complex, South Africa

HARTWIG E. FRIMMEL, DENNIS HOFFMANN, RON T. WATKINS*
Department of Geological Sciences, University of Cape Town, Rondebosch 7700, South Africa
JOHN M. MOORE
Department of Geology, Rhodes University, Grahamstown 6140, South Africa

ABSTRACT

Micas with variable Ba content in the interlayer sites occur in silicate-rich bands within the high-grade, metamorphic banded iron formation enclosing massive sulfide bodies in the Broken Hill deposit, Namaqualand Metamorphic Complex, South Africa. In those layers that contain neither potassium feldspar nor muscovite, a green, barian (up to 17 wt% BaO), trioctahedral mica occurs that is similar to kinoshitalite. In contrast to the originally described kinoshitalite, however, this mica is Fe-rich (average $X_{Fe} = 0.65$), suggesting the existence of an Fe analogue of kinoshitalite not described to date. Ion chromatographic analysis indicates that about 8% of the total Fe in this mica is present as Fe^{3+}, and a typical formula is $(Ba_{1.2}K_{0.4})(Fe^{2+}_{3.2}Mn_{0.2}Mg_{2.0}Al_{0.2}Fe^{3+}_{0.1}Ti_{0.2})(Al_{3.0}Si_{5.0})O_{20}(OH_{1.8}F_{2.2})$. The unit-cell parameters were determined as follows: $a = 5.383(2)$, $b = 9.328(8)$, $c = 10.055(8)$ Å, $\beta = 100.44(5)°$, with $V = 496.5$ Å^3, and $Z = 2$. The space group is $C2/m$. The Ba-rich mica formed at the peak of metamorphism ($T = 670 \pm 20$ °C, $P = 4.5 \pm 1.0$ kbar) at a pH below the muscovite + potassium feldspar buffer, f_{O_2} buffered by quartz + fayalite + magnetite and f_{S_2} between 10^{-5} and 10^{-7}.

INTRODUCTION

The banded iron formation interstratified with massive sulfide layers in the Broken Hill ore bodies near Aggeneys in the northern Cape Province, South Africa, contains Fe-rich mica with up to 17 wt% BaO. Compositionally, this mica is comparable to kinoshitalite, $BaMg_3Al_2Si_2O_{10}(OH)_2$, but has considerable substitution of Fe for Mg ($X_{Mg} \leq 0.3$). It appears that, similar to the phlogopite-annite series, solid solution exists between kinoshitalite and an Fe analogue of kinoshitalite. Kinoshitalite was defined by Yoshii et al. (1973a) as the Ba and Mg trioctahedral brittle mica. Nearly end-member kinoshitalite was described by Dasgupta et al. (1989), who also documented a complete solid solution between the K (phlogopite) and the Ba (kinoshitalite) end-members. Kinoshitalite containing considerable amounts of K was also reported by Solie and Su (1987), and potassic kinoshitalite with high Mn contents was described by Yoshii et al. (1973b), Yoshii and Maeda (1975), and Matsubara et al. (1976). Recently, the X-ray structure of Ba-rich trioctahedral micas has been refined by Brigatti and Poppi (1993), who also summarized the previous literature on the different occurrences of barian micas in metamorphic and igneous rocks. The Fe equivalent to kinoshitalite has not been reported to date.

In this paper we describe the mode of occurrence of an Fe-rich equivalent to kinoshitalite and its compositional characteristics as determined by electron probe microanalysis, ion chromatography, and X-ray diffraction. The possible origin of this unusual mineral and its bearing on the composition of metamorphic fluids in the vicinity of a massive sulfide deposit are discussed.

GEOLOGICAL SETTING

The Broken Hill ore bodies near Aggeneys, South Africa, represent a metamorphosed stratiform Pb-Zn-Cu-Ag sulfide deposit situated in the mid-Proterozoic supracrustal sequence of the Bushmanland Subprovince in the Namaqualand Metamorphic Complex (NMC). This sequence overlies a 2020 m.y.-old basement of augen gneiss and has at its base a thick series of leucogneisses, which have been interpreted as metarhyolite (Moore, 1989). The basal series is succeeded by metapelites (which are locally highly aluminous), massive quartzite, iron formation, and associated massive sulfide lenses. Above these lie a succession of metaconglomerates, gray gneisses, and amphibolites. The amphibolites, which are tholeiitic in character, have been dated at 1650 Ma (Reid et al., 1987). Peraluminous rocks intercalated within the metapelites (Willner et al., 1990) and associated B-rich exhalatives (Willner, 1992) are thought to have formed near hydrothermal vents during an intermediate stage of rifting that characterized the deposition of the Bushmanland Sequence. This event preceded the formation of the strati-

* Present address: School of Applied Geology, Curtin University, GPO Box U1987, Perth 6001, Western Australia.

0003–004X/95/0708–0833$02.00

form base-metal sulfide horizons, which have been equated with Sedex-type deposits (Ryan et al., 1986).

The ore bodies contain pyrrhotite, galena, sphalerite, chalcopyrite, and pyrite in decreasing order of abundance. They are enclosed by alternating magnetite-rich and manganiferous silicate-rich bands, with garnet- and amphibole-rich layers occurring within the latter. The silicate-rich bands contain the Ba-rich micas described here. Steep geochemical gradients are preserved on a millimeter scale between the iron formation and sulfide bands, indicating that only very limited element transfer took place across the lithological boundaries during metamorphism (Frimmel et al., 1993). Accordingly, the geochemistry of the iron formation bands is believed to be representative of the original depositional environment. The silicate-rich bands have compositions similar to chemical precipitates from modern submarine hydrothermal fluids, and the garnet- and amphibole-rich bands are interpreted as evolved and immature hydrothermal sediments, respectively. The latter originated through rapid precipitation after exhalation, whereas the former resided longer in the seawater before being deposited in more oxidizing environments distant from the hydrothermal vents (Frimmel et al., 1993; Hoffmann, 1994).

The Bushmanland Sequence was subjected to upper amphibolite to granulite facies metamorphism during the 1.1 Ga Namaqualand metamorphic event (Waters, 1989). In the Aggeneys area, metapelites contain the equilibrium assemblage muscovite + biotite + sillimanite + quartz + garnet + magnetite ± potassium feldspar ± graphite ± sulfides. Coexistence of muscovite + biotite + sillimanite + potassium feldspar + quartz, together with the absence of migmatites, constrains the peak metamorphic *P-T* conditions at 4.5 ± 1.0 kbar and 670 ± 20 °C. Garnet + biotite and garnet + cordierite thermometry yields temperatures that are in good agreement with these estimates (Waters, 1989).

Analytical procedures

Compositions of the micas and associated minerals were determined using a Cameca (Camebax) electron microprobe at 15 kV accelerating voltage and 2 μm electron-beam diameter. Mica analyses were double-checked with the electron beam defocused to 5 μm. The counting time was 10 s, except for Ba, Zn, F, and Cl, which were counted for 30 s. The standards used in the analysis of the micas were natural fluorite (F), scapolite (Cl), chromite (Cr), hornblende (Na, K, Si, Al, Fe, Mg, Ca), synthetic rhodochrosite (Mn), rutile (Ti), and Ba-Si glass (Ba). Concentrations were corrected by ZAF, except for Fe-rich analyses, which were corrected following the method of Bence and Albee (1968). Total Mn and total Fe were computed as MnO and FeO, respectively.

Mineral concentrates were obtained by use of a magnetic separator and final hand-picking under the microscope. Fe^{2+}/Fe^{3+} ratios were determined on pure mica concentrates using a Dionex 4000i ion chromatograph. The method used was a modification of that described by Kanai (1990) for the determination of Fe^{2+} and Fe^{3+}, with the Fe^{2+}/Fe^{3+} ratio determined by comparison with standard rock powders of known Fe-oxidation state (le Roex and Watkins, 1995). Fifty mg of mica, finely powdered under acetone, was dissolved by gentle heating with a $HF:H_2SO_4$ mix in a covered Pt crucible. The dissolved sample was diluted with de-oxygenated, de-ionized water and 50 μL injected onto a Dionex CS-5 separator column coupled to CG-5 guard column. The sample was eluted with 6 m*M* pyridine-2 6-dicarboxylic acid (PDCA), and the iron species were detected using a UV-VIS variable wavelength detector at 520 nm after postcolumn reaction with a broad metal complexing agent 4-(2-pyridylazo) resorcinol (PAR). Individual mica concentrates were analyzed a minimum of three times until highly consistent results were obtained, thereby eliminating occasional aberrant values that may result from imperfect sample preparation. The Fe^{2+}/Fe^{3+} ratio was measured by direct comparison of the ratio of the individual peak heights with those obtained from similar analysis of certified rock standard W-2 (le Roex and Watkins, 1995).

Powdered concentrates of the micas were analyzed at the University of Cape Town, using standard X-ray diffractometry techniques with a Cu$K\alpha$ radiation of 40 kV and 30 mA. An automatic divergence slit was used and counts were recorded for individual steps of 0.02° 2θ size and a counting time of 2 s per step. Single crystals were studied at the Institute of Mineralogy and Crystallography, University of Vienna, using both single-crystal photography and a Stoe four-circle diffractometer AED2 and graphite-monochromatic Mo$K\alpha$ radiation. The operating conditions were as follows: 40 steps per reflection, increased for $\alpha_1 - \alpha_2$ splitting; 0.03° and 0.5–2.0 s per step; 2 × 4 steps for background measurement; 3 standard reflections each 120 min; and $2\theta_{max} = 60°$. Structure refinement was obtained with the SHELXL-93 package of programs.

Paragenesis

The mineral assemblages in the iron formation at Aggeneys containing the Ba-rich mica are quartz + magnetite + garnet + apatite ± sillimanite ± gahnite ± sulfides, with amphibole + olivine ± pyroxferroite additionally present in amphibole-rich layers. The Ba-rich micas occur in textural equilibrium with quartz, magnetite, garnet, and amphibole. The garnets are essentially solid solutions between almandine and spessartine. Considerable variation in X_{Sps} exists between different rock types and also within individual iron formation bands. There is a steep gradient from high X_{Sps} (up to 62 mol%) in the iron formation bands close to the massive sulfide bodies to low X_{Sps} (down to 9 mol%) in the ferruginous quartzites and pelites further away from the ore lenses. Similar variations were found in the compositions of the amphiboles, most of which are grunerites with variable amounts of Mn and Mg. Those in the amphibole-rich iron formation bands have the highest Mn contents, with an average formula of $Na_{0.17}Mn_{0.80}Fe^{2+}_{4.1}Mg_{1.4}Fe^{3+}_{0.51}(Al_{0.21}$-

TABLE 1. Representative electron microprobe analyses of biotite from various rock types around the massive sulfide bodies

Sample	HFN40	HFN41	HFN44	HFN45	HFN47	TS12	TS3
SiO_2	34.78	37.90	32.38	34.94	36.16	40.74	40.23
TiO_2	4.01	2.03	3.43	2.09	0.84	0.17	0.00
Al_2O_3	19.24	19.85	17.24	20.26	16.37	12.66	15.12
Cr_2O_3	0.00	0.00	0.00	0.00	0.00	0.00	0.00
FeO*	24.29	13.19	29.82	24.81	14.82	11.67	14.20
MnO	0.24	1.40	0.62	0.00	0.27	0.48	0.71
MgO	5.61	13.18	4.55	5.77	15.62	19.25	15.94
CaO	0.00	0.00	0.00	0.00	0.00	0.00	0.00
Na_2O	0.16	0.13	0.00	0.20	0.26	0.29	0.28
K_2O	9.23	6.57	7.30	9.24	8.08	8.92	8.00
F^-	0.00	2.32	0.00	0.00	3.72	5.92	4.90
Cl^-	0.13	0.00	0.00	0.00	0.00	0.00	0.00
BaO	0.29	0.97	2.25	0.45	3.72	0.00	0.00
SrO	0.18	0.20	0.18	0.19	0.17	0.00	0.00
Total	98.13	96.76	97.77	97.95	98.46	97.61	97.32
Si	5.29	5.54	5.16	5.32	5.48	6.02	5.95
$^{[4]}Al$	2.71	2.46	2.84	2.68	2.52	1.98	2.05
$^{[6]}Al$	0.74	0.96	0.39	0.96	0.40	0.22	0.58
$^{[6]}Ti$	0.46	0.22	0.41	0.24	0.10	0.02	0.00
Fe^{2+}	3.09	1.61	3.97	3.16	1.88	1.44	1.76
Mn^{2+}	0.03	0.17	0.08	0.00	0.03	0.06	0.09
Mg	1.27	2.87	1.08	1.31	3.53	4.24	3.51
K	1.79	1.23	1.48	1.80	1.56	1.68	1.51
Na	0.05	0.04	0.00	0.06	0.08	0.08	0.08
Ba	0.02	0.06	0.14	0.03	0.22	0.00	0.00
Sr	0.02	0.02	0.02	0.02	0.02	0.00	0.00
F	0.00	1.07	0.00	0.00	1.78	2.77	2.29
Cl	0.03	0.00	0.00	0.00	0.00	0.00	0.00

Note: HFN40 and HFN45 = pelite, HFN41 and TS12 = massive sulfide ore, HFN44 and HFN47 = garnet-quartzite, TS3 = banded iron formation. Normalization based on 22 $O_{equivalent}$; totals corrected for F, Cl = O equivalency.

* All Fe reported as FeO.

TABLE 2. Representative electron microprobe analyses of muscovite from various rock types associated with massive sulfide bodies

Sample	HFN41	HFN44	HFN45	HFN47	HFN46
SiO_2	43.92	44.23	45.20	43.71	44.31
TiO_2	1.68	0.99	1.23	1.54	1.53
Al_2O_3	32.75	33.79	34.08	34.68	34.15
Cr_2O_3	0.00	0.00	0.00	0.00	0.00
FeO*	1.41	5.32	2.50	1.74	1.88
MnO	0.00	0.00	0.00	0.12	0.13
MgO	1.70	1.04	0.66	1.98	2.02
CaO	0.00	0.00	0.00	0.00	0.00
Na_2O	0.32	0.00	0.33	0.19	0.19
K_2O	9.86	6.14	10.34	4.62	4.61
F^-	0.00	0.00	0.00	1.65	1.80
Cl^-	0.03	0.00	0.00	0.00	0.00
BaO	1.96	3.76	0.54	5.56	4.89
SrO	0.26	0.25	0.25	0.19	0.26
Total	93.88	95.52	95.13	95.29	95.01
Si	6.06	6.04	6.11	5.98	6.05
$^{[4]}Al$	1.94	1.96	1.89	2.02	1.95
$^{[6]}Al$	3.39	3.48	3.54	3.57	3.55
$^{[6]}Ti$	0.17	0.10	0.13	0.16	0.16
Fe^{2+}	0.16	0.61	0.28	0.20	0.21
Mn^{2+}	0.00	0.00	0.00	0.01	0.02
Mg	0.35	0.21	0.13	0.40	0.41
K	1.74	1.07	1.78	0.81	0.80
Na	0.09	0.00	0.09	0.05	0.05
Ba	0.11	0.20	0.03	0.30	0.26
Sr	0.02	0.02	0.02	0.02	0.02
F	0.00	0.00	0.00	0.71	0.78
Cl	0.01	0.00	0.00	0.00	0.00

Note: for rock types see Table 1. HFN46 = massive sulfide rock. Totals corrected for F, Cl = O equivalency.

* All Fe reported as FeO.

$Fe^{3+}_{0.12}Si_{7.67}O_{22})(OH)_2$. Olivine is restricted to amphibole-rich iron formation bands and is of the knebelite variety, with an average of 82.8 mol% fayalite, 16.3 mol% tephroite, and 2.9 mol% forsterite. Orthopyroxene is manganoan ferrosilite with an average formula of $Fe_{1.46}Mn_{0.28}Mg_{0.26}Al_{0.01}Si_{1.99}O_{6.00}$. It occurs rarely in the amphibole-rich bands, where pyroxferroite of average composition $Fe_{0.95}Mn_{0.93}Mg_{0.11}Si_{2.00}O_{6.00}$ is more common. The gahnite is ferroan and its composition depends on the host rock: X_{Gahn} = 0.46–0.69, X_{Hc} = 0.19–0.49, and X_{Spl} = 0.02–0.05. The Zn content of the spinel decreases abruptly away from the ore bodies.

Biotite with light- to dark-brown pleochroism and colorless muscovite may be distinguished within the massive sulfide bodies and enclosing banded iron formation, quartzites, and pelites. Representative analyses of biotite from the various rock types are given in Table 1. The biotite contains up to 3.7 wt% BaO and 0.2 wt% SrO. The F content ranges from below the detection limit (0.16 wt%) to 5.9 wt%. Cl contents are below the detection limit (0.025 wt%) except in sample HFN40, a pelite, with 0.13 wt% Cl in the biotite. Variation in the intensity of color and pleochroism is largely because of a variation in TiO_2 contents, which range from below the detection limit (0.04 wt%) to 4.0 wt%.

Muscovite is restricted to the massive sulfide bodies, pelites, and quartzites. Representative analyses of muscovite, given in Table 2, are of samples coexisting with the biotite listed in Table 1. Increased Ba, Sr, Ti, and F contents in the biotite are similarly reflected in elevated concentrations of the same elements in the coexisting muscovite. The latter contains up to 5.6 wt% BaO, 0.3 wt% SrO, and up to 1.7 wt% TiO_2. Few samples are rich in Ba and contain both muscovite and biotite but no potassium feldspar. In these few samples, the distribution of Ba between muscovite and coexisting biotite is regular (Fig. 1). Partition coefficients describing the fractionation of Ba and K between muscovite and biotite were calculated: K_D [=$(Ba/K)_{Bt}/(Ba/K)_{Ms}$)] ranges between 0.38 in garnet quartzite and 0.77 in massive sulfide ore. F contents are below the detection limit (0.16 wt%) in most samples, but up to 1.8 wt% F was found in muscovite from a massive sulfide lens that contains no biotite.

A third, green variety of mica occurs exclusively in the silicate-rich bands within the iron formation, where it is localized particularly in association with garnet-rich bands. This mica forms subhedral laths up to 0.2 mm long. It is characterized by a high BaO content of up to 17.0 wt% and is described in detail below.

CHARACTERISTICS OF THE Ba-RICH MICAS

The Ba-rich mica variety displays, like all other micas, a perfect {001} cleavage. The grains are strongly pleochroic (X = grass green, Y = dark brown green, Z = dark greenish gray-brown); absorption is $X \ll Z < Y$; and the

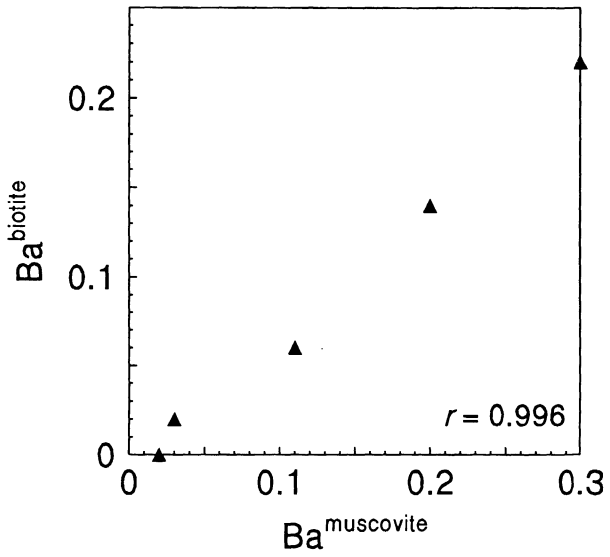

Fig. 1. Atomic content of Ba in muscovite plotted against that in biotite. The data points represent average values obtained for samples that contain both micas in textural equilibrium.

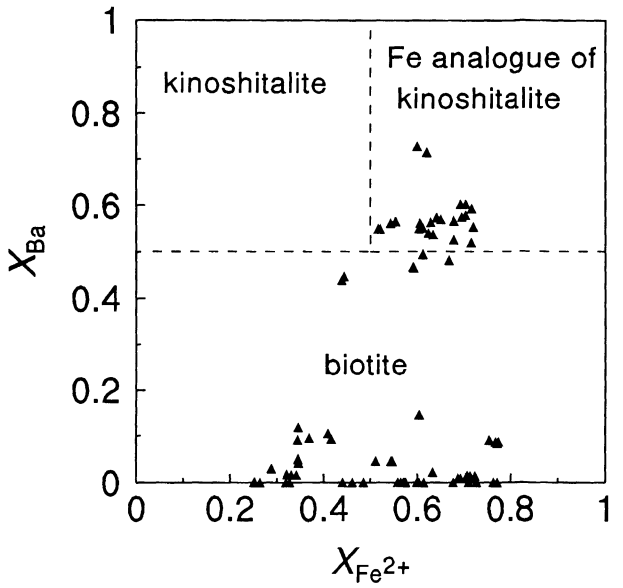

Fig. 2. X_{Ba} vs. $X_{Fe^{2+}}$ diagram for biotite and the barian trioctahedral micas analyzed. Note that most of the latter have $X_{Fe^{2+}}$ values >0.5 and are therefore described as Fe analogue of kinoshitalite.

refractive index $\beta = 1.680$. The strong characteristic color of this mineral inhibits the determination of the birefringence in a thin section, but it appears similar to biotite. The optic character is biaxial negative. Dispersion is very weak, and $2V_\alpha$ is around 20°. Representative compositions of this mineral are given in Table 3. On the basis of the Ba/(Ba + K + Na) ratio, which is as high as 0.73, this mica approaches the composition of kinoshitalite. It contrasts, however, with originally described kinoshitalite (Yoshii et al., 1973a), a Mg-phase, by having X_{Fe} [=Fe/(Fe + Mg)] values of up to 0.72 (Fig. 2). Thus the mica can be described as a solid solution between kinoshitalite and an Fe analogue of kinoshitalite. Most of the green micas described here have $X_{Fe} > 0.5$ and are therefore Fe analogues of kinoshitalite.

TABLE 3. Representative electron microprobe analyses of Ba-rich biotite and Fe analogue of kinoshitalite

Sample	HFN42	HFN42	HFN43	HFN43	189113	TS8
SiO_2	28.54	28.04	28.72	29.98	28.49	30.43
TiO_2	1.72	2.74	2.43	2.34	1.40	1.79
Al_2O_3	14.32	14.05	15.32	15.24	15.71	15.93
Cr_2O_3	0.00	0.00	0.00	0.00	0.00	0.00
Fe_2O_3	2.14	2.21	2.32	2.31	2.12	2.15
FeO	22.20	22.84	23.96	23.86	21.98	22.28
MnO	1.14	1.53	1.09	1.16	1.33	0.41
MgO	7.42	5.77	6.34	6.59	7.81	8.37
CaO	0.00	0.00	0.00	0.00	0.00	0.00
Na_2O	0.20	0.18	0.23	0.20	0.06	0.30
K_2O	3.20	3.08	3.45	3.87	1.94	3.20
F^-	3.70	2.91	2.19	2.45	4.02	3.38
Cl^-	0.00	0.00	0.00	0.00	0.00	0.00
BaO	13.90	14.25	13.73	12.66	16.95	12.99
SrO	0.14	0.00	0.00	0.00	0.00	0.00
Total	97.06	96.37	98.86	99.63	100.09	99.79
Si	5.09	5.07	5.00	5.12	4.98	5.13
$^{[4]}Al$	2.91	2.93	3.00	2.88	3.02	2.87
$^{[4]}Ti$	0.00	0.00	0.00	0.00	0.00	0.00
$^{[6]}Al$	0.10	0.06	0.14	0.19	0.21	0.29
$^{[6]}Ti$	0.23	0.37	0.32	0.30	0.18	0.23
Fe^{3+}	0.10	0.11	0.11	0.11	0.10	0.10
Fe^{2+}	3.31	3.45	3.49	3.41	3.21	3.14
Mn^{2+}	0.17	0.23	0.16	0.17	0.20	0.06
Mg	1.97	1.55	1.64	1.68	2.03	2.10
K	0.73	0.71	0.77	0.84	0.43	0.69
Na	0.07	0.06	0.08	0.07	0.02	0.10
Ba	0.97	1.01	0.94	0.85	1.16	0.86
Sr	0.01	0.00	0.00	0.00	0.00	0.00
F	2.09	1.66	1.21	1.32	2.22	1.80

Note: Fe^{3+}/Fe^{2+} ratio as derived from ion chromatography. Normalization based on 22 $O_{equivalent}$; totals corrected for F, Cl = O equivalency.

The Fe analogue of kinoshitalite from Aggeneys is not only more ferrous but also less aluminous than kinoshitalite, with Al:Si of approximately 0.6 rather than 1.0 in kinoshitalite. The Al-free end-member of the corresponding solid-solution series is anandite, $BaFe_3(Si,Fe)_4(O,OH)_{10}(OH,S,Cl)$. An additional substitution found in the Fe analogue of kinoshitalite from Aggeneys is that of F for OH. With F concentrations of up to 4.1 wt%, the F/(F + OH) ratio is as high as 0.6. The F content can vary considerably between 1 and 2.6 F atoms per formula unit. The range in F content in the barian biotite from the surrounding rock types is even greater (between 0 and 3 F atoms per formula unit) with no apparent correlation between F and Ba (Fig. 3). Poor negative correlations are evident between F and X_{Fe}, and F and $^{[6]}Al$ (Fig. 4). The former accords with the well-established F-Fe avoidance rule (Valley et al., 1982; Guidotti, 1984), and the latter confirms a similar F-$^{[6]}Al$ avoidance already suspected by Guidotti (1984). The low degree of correlation can be explained by the influence of other variables, notably the X_{Fe} of the whole rock, f_{O_2}, f_{S_2}, and f_{HF}, which varied considerably between the different rock types (Frimmel et al., 1993).

A series of exchange components can be constructed

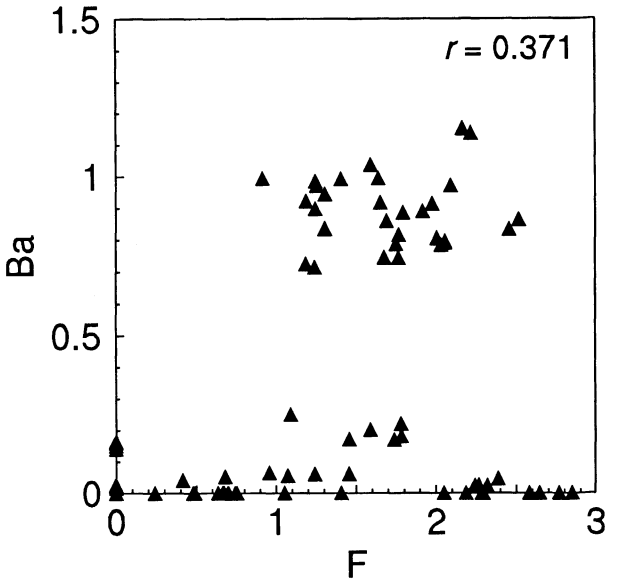

Fig. 3. Atomic content of F plotted against Ba in Ba-poor and in Ba-rich biotite and an Fe analogue of kinoshitalite from the Broken Hill deposit.

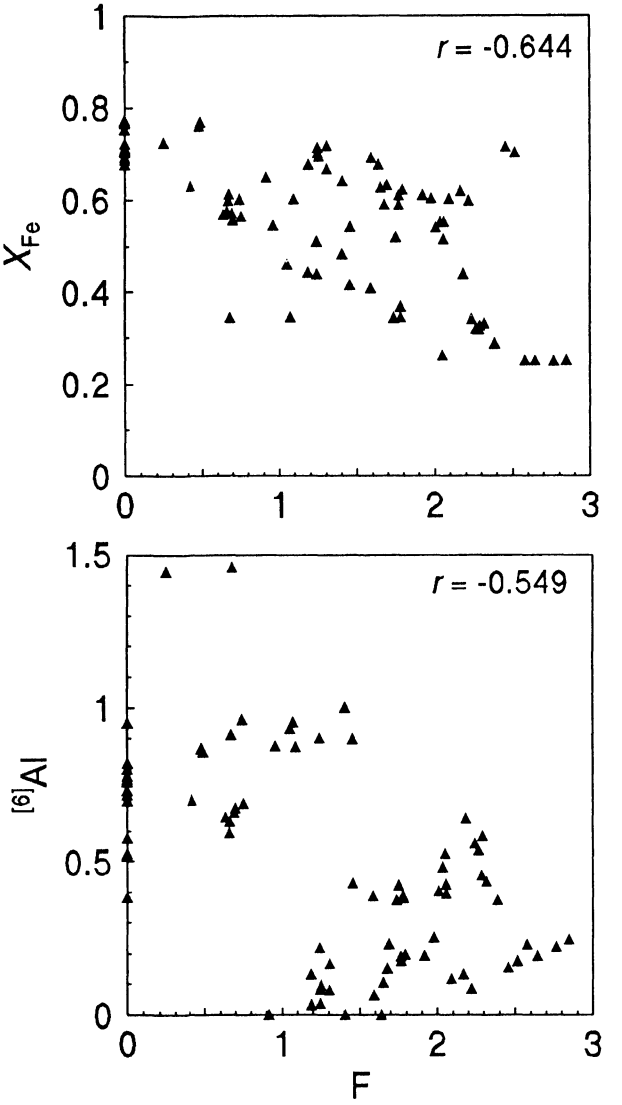

Fig. 4. Atomic content of F plotted against X_{Fe} [=Fe^{2+}/(Fe^{2+} + Mn + Mg)] (**top**) and $^{[6]}$Al (**bottom**) of the biotite from the Broken Hill deposit. The poor but noticeable correlations suggest not only an Fe-F but also an $^{[6]}$Al-F avoidance.

for the barian biotite and for kinoshitalite (Tracy, 1991). The exchange vectors include the interlayer, coupled with tetrahedral, substitutions (1) $BaAlK_{-1}Si_{-1}$, (2) $BaFe^{3+}$-$K_{-1}Si_{-1}$, (3) NaK_{-1}, (4) $SrAlK_{-1}Si_{-1}$; octahedral substitutions (5) $FeMg_{-1}$, (6) $TiAl_2Mg_{-1}Si_{-2}$, (7) $R^{3+}_2\square Mg_{-3}$, (8) $R^{3+}_2Mg_{-1}Si_{-1}$; tetrahedral substitutions (9) $Fe^{3+}Al_{-1}$, and the anion substitution (10) $F(OH)_{-1}$. The exchange vectors (1) and (3) are supported by the sympathetic variation of (K + Na + Si) with (Ba + $^{[4]}$Al) (Fig. 5). The barian micas from Aggeneys do not show good correlation between Ba and Al_{tot} (Fig. 6A) as described by Tracy (1991) for barian micas from the Franklin Marble, New Jersey. The micas in this study, however, show strong correlation between [K^+ + $3(Mg,Fe)^{2+}$ + $3Si^{4+}$] and (Ba^{2+} + $2Ti^{4+}$ + $3Al^{3+}$) ($r = -0.987$) (Fig. 6B), which supports the combination of the exchange vectors (1), (6), and $Ti\square(Fe,Mg)_{-2}$ as proposed by Mansker et al. (1979). These combined substitutions introducing Ba should increase Al_{tot}, but this is not supported by our data (Fig. 6A). An additional substitution, such as $Fe^{2+}Fe^{3+}_3SiMg_{-3}Al_{-2}$, reflecting the kinoshitalite-anandite join, is required to explain our data.

Using Mössbauer spectroscopy Guidotti and Dyar (1991) determined that biotite from different silicate mineral assemblages and metamorphic grades has 8 ± 3% of Fe_{tot} as $^{[4]}Fe^{3+}$, and that in biotite coexisting with magnetite 10–13% of Fe_{tot} occurs as $^{[6]}Fe^{3+}$, whereas in biotite coexisting with graphite 4% of Fe_{tot} occurs as $^{[6]}Fe^{3+}$. New data reported by Swope et al. (1994) indicate, however, that $^{[4]}Fe^{3+}$ contents are negligible, and thus quoted Fe^{3+} contents are essentially $^{[6]}Fe^{3+}$ contents. Magnetite is stable over a wide range of f_{O_2}. The micas of the present study locally coexist not only with magnetite but also with sulfides. On the basis of charge-balance criteria and site allocation, there is no necessity for any Fe to be present as Fe^{3+}. We attempted to quantify the Fe^{3+}/Fe^{2+} ratio in representative biotite and samples of the Fe-analogue of kinoshitalite using ion chromatographic analysis. Repeated analysis of essentially Ba-free biotite from pelites (samples HFN40 and HFN45, Table 1) revealed that 6 and 4%, respectively, of Fe_{tot} occurs as Fe^{3+}. The results for the Fe analogue of kinoshitalite (sample HFN42, Table 3) indicate that, on average, 8% of Fe_{tot} is present as Fe^{3+}. This reflects a degree of Fe-oxidation that is in good agreement with the results recently obtained on synthetic annite (Rancourt et al., 1994). Taking this Fe^{3+}/Fe^{2+} ratio as representative for the Fe analogue of kinoshitalite, a typical formula for this mica would be $(Ba_{1.2}K_{0.4})$-$(Fe^{2+}_{3.2}Mn_{0.2}Mg_{2.0}Al_{0.2}Fe^{3+}_{0.1}Ti_{0.2})(Al_{3.0}Si_{5.0})O_{20}(OH_{1.8}F_{2.2})$.

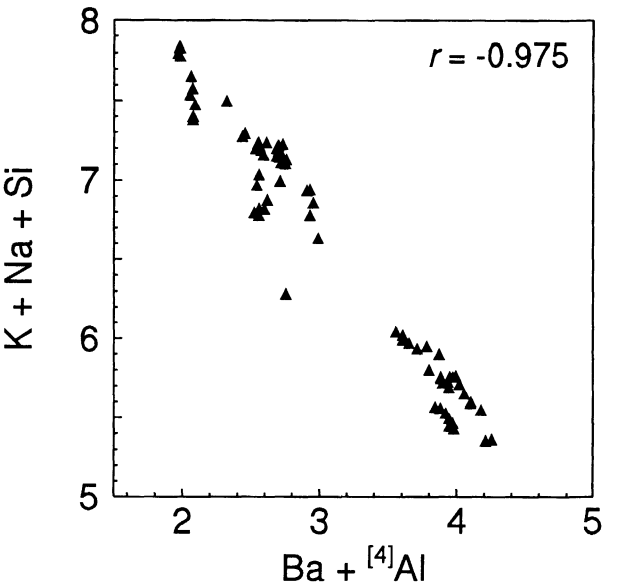

Fig. 5. Ba + [4]Al plotted against K + Na + Si of the Ba-rich and Ba-poor micas from the Broken Hill deposit.

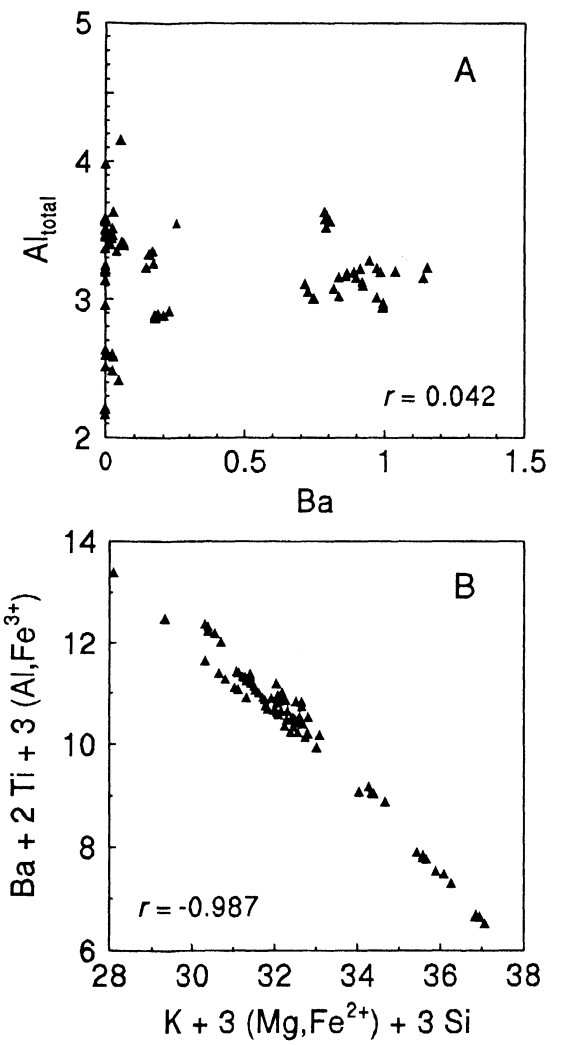

Fig. 6. (**A**) Al_{tot} vs. Ba diagram, (**B**) [K + 3(Mg,Fe^{2+}) + 3Si] plotted against [Ba + 2Ti + 3(Al,Fe^{3+})] of the Ba-rich and Ba-poor micas from the Broken Hill deposit.

X-ray diffraction of a powder comprising 99% pure Fe analogue of kinoshitalite yielded six well-defined reflections and six poorly defined reflections. The main peaks represent 001 basal reflections because of the preferred orientation of the individual particles in the sample. The 00*l* peak positions and relative intensities match very well with those of the $2M_1$ polytype of anandite. The positions of the weak 0*kl*, *k*0*l*, and *hkl* reflections, however, are not in agreement with those of anandite and match better those of kinoshitalite. Single-crystal photography of five selected grains yielded very consistent results, which indicate a 1*M* structure for this mica. The refined unit-cell parameters from a total of 3075 measured reflections are as follows: $a = 5.383(2)$, $b = 9.328(8)$, $c = 10.055(8)$ Å, $\beta = 100.44(5)°$, with $V = 496.5$ Å^3, and $Z = 2$. The space group choice is *C*2/*m*.

Genesis of Ba-rich micas

The geochemistry of the silicate-rich iron formation bands hosting the Ba-rich micas is consistent with a hydrothermal to hydrogenous origin (Frimmel et al., 1993; Hoffmann, 1994). The most likely depositional environment for the banded iron formation and the associated Sedex-type massive sulfide bodies is a rift-related basin. Evidence for this comes from the relative thinness of the supracrustal sequence (<3 km), the preservation of undisturbed millimeter scale banding indicative of a quiet depositional environment, and the geochemistry of the mafic rocks in the sequence (Reid et al., 1987). Ba enrichment in metalliferous sediments on the seafloor has been documented in numerous areas in proximity to hydrothermal activity, such as oceanic ridges. Haymon and Kastner (1981), for instance, reported particulate barite together with amorphous silica from white smoker chimney edifices on seafloor basalts. In addition to the precipitation as barite, Ba may be concentrated by substitution into clays and zeolites and by adsorption into Fe-Mn oxide particles. Additional terrigenous Ba could be contributed by detrital Ba-bearing feldspars.

During diagenesis and subsequent metamorphism, detrital feldspars, clays, and zeolites become unstable. Ba present in these phases is released and re-incorporated in metamorphic minerals, such as micas and feldspars. The most important Ba precursor mineral, particularly in a hydrothermal environment, is believed to be barite. Barite can remain stable up to granulite facies metamorphic conditions (Grew et al., 1991), depending upon the prevailing $f_{O_2} - f_{S_2}$ conditions.

The alternation of Fe-oxide- and Fe-sulfide-rich layers documents the preservation of geochemical gradients with respect to $f_{O_2} - f_{S_2}$. Systematic variations in the composition of garnet, amphibole, olivine, and micas across

the massive sulfide bodies and their surroundings also indicate that the exchange of elements such as Fe, Mg, and Mn across lithological boundaries was minimal despite the high grade of metamorphism (Frimmel et al., 1993). Green, coarse-grained, Pb-bearing amazonite is present only locally, along contact zones a few centimeters thick between metapelite and massive sulfide horizons. This indicates a strong gradient in f_{S_2} between sulfide and silicate layers.

Steep gradients in f_{HF} are documented by the highly variable F contents in micas and apatite. Following Gunow et al. (1980), $\log(f_{H_2O}/f_{HF})$ was calculated on the basis of the F intercept value for biotite. Similarly, $\log(f_{H_2O}/f_{HF})$ was calculated from apatite using the thermodynamic data of Zhu and Sverjensky (1991). For the surrounding metapelites, these values are in the range between 3.5 and 4.3, which is in agreement with the findings in amphibolite-granulite transition zones elsewhere (Yardley, 1985; Nijland et al., 1993). Within the banded iron formation, dramatic variations in (f_{H_2O}/f_{HF}) were found with f_{HF} being increased by up to four orders of magnitude.

The occurrence of the Fe analogue of kinoshitalite described here is confined to iron formation bands for which anomalous high f_{HF} values were obtained. The same bands lack potassium feldspar, which can be explained by a low pH in the peak metamorphic fluid, as indicated by the high f_{HF}. In the absence of potassium feldspar, the micas became the dominant sinks for Ba. Thus it appears that the major factors controlling the formation of the Ba-rich micas include original whole rock composition, pressure, temperature, pH, f_{O_2}, and f_{S_2}. The pH must be below the muscovite + potassium feldspar buffer, which is around 5.8 at the given P-T conditions (4.5 kbar and 670 °C) and $a_{K^+} = 0.1$. Within the horizon containing the Fe analogue of kinoshitalite, $\log f_{O_2}$ is buffered at -17.3 by quartz + fayalite + magnetite (Fig. 7). The predominance of pyrrhotite in the associated massive sulfide bodies indicates $\log f_{S_2} < -1$ in the sulfide horizons. Only locally was pyrrhotite found together with pyrite in the massive sulfide bodies. The breakdown of barite in the silicate layers may be approximated by the reaction 2barite = $2Ba^{2+}_{in\ mica} + S_2 + 4O_2$ for which log K was calculated as -64.8 at the given P-T conditions, on the basis of the thermodynamic data of Johnson et al. (1992). The Ba^{2+} activity is directly proportional to f_{S_2}, and a minimum $\log f_{S_2}$ of -7 can be calculated for an assumed $a_{Ba^{2+}}$ of 0.1. Thus the ambient $\log f_{S_2}$ in the silicate layers containing the Fe analogue of kinoshitalite must have been between -4 and -7 at the f_{O_2} conditions outlined above (Fig. 7).

Ba partitions into silicate phases in the following sequence: potassium feldspar > muscovite > biotite. Provided the pH is below the muscovite + potassium feldspar buffer, a further requirement for the formation of the Fe analogue of kinoshitalite is the absence of muscovite. Because of the preferential partitioning of Ba into muscovite, Ba contents in any coexisting biotite would be lower, probably too low for the formation of a kinoshitalite.

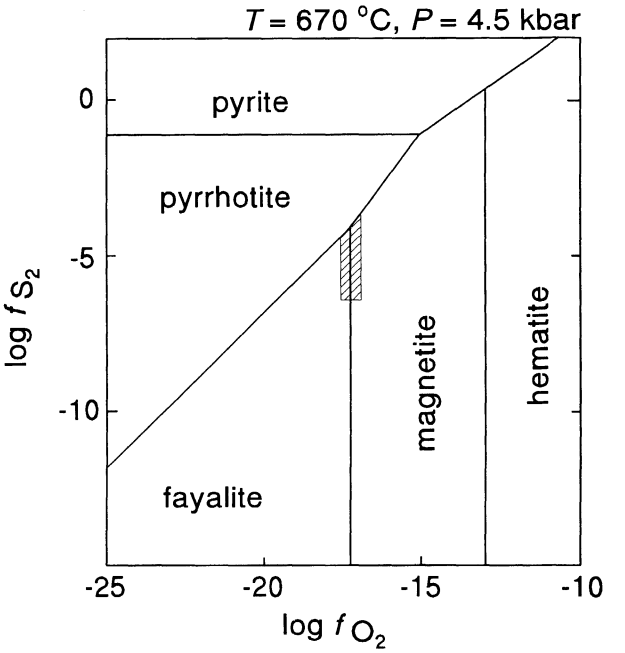

Fig. 7. Log f_{O_2} − log f_{S_2} diagram showing the stability of pyrite, pyrrhotite, fayalite, magnetite, and hematite (+ quartz) in the Fe-O-S-SiO_2 system at the peak metamorphic conditions estimated for the Broken Hill deposit. The hatched area indicates the most likely conditions for the formation of iron kinoshitalite. Thermodynamic standard-state data used are from Johnson et al. (1992).

Conclusions

The compositional characteristics of the micas from the Broken Hill deposit suggest that the group of trioctahedral brittle Ba-bearing micas comprises not only kinoshitalite and anandite but also an Fe-analogue of kinoshitalite. Complete solid solution seems to exist between the kinoshitalite and the Fe-analogue of kinoshitalite and their respective F-bearing equivalents. The gap between the data fields for the less barian and more barian micas in Figures 3 and 6A suggests the possible presence of immiscibility between the phlogopite-annite series and the join between kinoshitalite and its Fe analogue.

Ba-rich micas from both igneous and metamorphic rocks have been described. These include manganoan varieties in Mn-oxide-rich rocks from the Noda-Tamagawa mine (Yoshii et al., 1973b), from Hokkejino, Japan (Matsubara et al., 1976), and from the Sausar Group at Netra, India (Dasgupta et al., 1989). In the latter example, kinoshitalite occurs in rocks that have experienced metamorphism (650 °C, 6 kbar) similar to that of the rocks described here, but Dasgupta et al. (1989) ascribed the formation of kinoshitalite to the infiltration of postmetamorphic pegmatitic and CO_2-rich hydrothermal fluids. Solie and Su (1987) described Mn-poor kinoshitalite from contact metamorphosed calcareous metasedimentary rocks in the Alaska Range and also concluded that kinoshitalite formed at high temperatures (≥600 °C) but not necessarily at high pressure. It thus appears from these

studies and the present work that the formation of barian micas in metamorphic rocks is favored by high temperatures (>600 °C). The role of pressure remains unknown. Grapes (1993) explained a Ba-enrichment of muscovite in Ba-rich metacherts by high f_{S_2}, as indicated by the presence of sulfides and a correspondingly low oxidation state. Our results confirm this trend also for barian biotite, kinoshitalite, and its Fe analogue.

Acknowledgments

The results presented here emerged from a project that was funded by Gold Fields of South Africa. The authors are grateful to the following for their cooperation and support in this study: F. Pertlik, University of Vienna, for single-crystal photography and diffractometry; R.S. Rickard for microprobe assistance; and S. Horwood for help with the ion chromatographic analysis. Constructive reviews by R.F. Dymek and E. Grew greatly improved the manuscript.

References cited

Bence, A.E., and Albee, A.L. (1968) Empirical correction factors for the electron microanalysis of silicates and oxides. Journal of Geology, 76, 382–403.

Brigatti, M.F., and Poppi, L. (1993) Crystal chemistry of Ba-rich trioctahedral micas-1*M*. European Journal of Mineralogy, 5, 857–871.

Dasgupta, S., Chakraborti, S., Sengupta, P., Bhattacharya, P.K., Banerjee, H., and Fukuoka, M. (1989) Compositional characteristics of kinoshitalite from the Sausar Group, India. American Mineralogist, 74, 200–202.

Frimmel, H.E., Hoffmann, D., and Moore, J.M. (1993) Preservation of syn-depositional geochemical characteristics of the Broken Hill massive sulphide deposits, South Africa, during upper ampibolite facies metamorphism. In P. Fenoch Hach-Ali, J. Torres-Ruiz, and F. Gervilla, Eds., Current research in geology applied to ore deposits, p. 303–306. University of Granada, Granada, Spain.

Grapes, R.H. (1993) Barian mica and distribution of barium in metacherts and quartzofeldspathic schists, Southern Alps, New Zealand. Mineralogical Magazine, 57, 265–272.

Grew, E.S., Yates, M., Swihart, G.H., Moore, P.B., and Marquez, N. (1991) The paragenesis of serendibite at Johnsburg, New York, USA: An example of boron enrichment in the granulite facies. In L.L. Perchuk, Ed., Progress in metamorphic and magmatic petrology, p. 247–285. Cambridge University Press, Cambridge, U.K.

Guidotti, C.V. (1984) Micas in metamorphic rocks. In Mineralogical Society of America Reviews in Mineralogy, 13, 357–467.

Guidotti, C.V., and Dyar, M.D. (1991) Ferric iron in metamorphic biotite and its petrologic and crystallochemical implications. American Mineralogist, 76, 161–175.

Gunow, A.J., Ludington, S., and Munoz, J.L. (1980) Fluorine in micas from the Henderson molybdenite deposit, Colorado. Economic Geology, 75, 1127–1137.

Haymon, R.M., and Kastner, M. (1981) Hot spring deposits on the East Pacific Rise at 21 °N: Preliminary description of mineralogy and genesis. Earth and Planetary Science Letters, 53, 363–381.

Hoffmann, D. (1994) Geochemistry and genesis of manganiferous silicate-rich iron formation bands in the Broken Hill deposit, Aggeneys, South Africa. Exploration and Mining Geology, 3, 407–418.

Johnson, J.W., Oelkers, E.H., and Helgeson, H.C. (1992) Supcrt92: A software package for calculating the standard molal thermodynamic properties of minerals, gases, aqueous species, and reactions from 1 to 5000 bar and 0 to 1000 °C. Computers and Geosciences, 18, 899–947.

Kanai, Y. (1990) Simultaneous determination of iron(II) and iron(III) oxides in geological materials by ion chromatography. Analyst, 115, 809–812.

le Roex, A.P., and Watkins, R.T. (1995) A rapid ion chromatographic method for the determination of the Fe^{3+}/Fe^{2+} ratio in silicate rocks and minerals. Geochemical Journal, 29, in press.

Mansker, W.L., Ewing, R.C., and Keil, K. (1979) Barian-titanian biotites in nephelinites from Oahu, Hawaii. American Mineralogist, 64, 156–159.

Matsubara, S., Kato, A., Nagoshima, K., and Matsuo, G. (1976) The occurrence of kinoshitalite from Hokkejino, Kyoto Prefecture, Japan. Bulletin of the Natural (National) Science Museum, Series C (Geology), 2, 71–78.

Moore, J.M. (1989) A comparative study of metamorphosed supracrustal rocks from the western Namaqualand Metamorphic Complex. Bulletin of the Precambrian Research Unit, 37, 370 p. University of Cape Town, Cape Town, South Africa.

Nijland, T.G., Jansen, J.B.H., and Maijer, C. (1993) Halogen geochemistry of fluid during amphibolite-granulite metamorphism as indicated by apatite and hydrous silicates in basic rocks from the Bamble Sector, South Norway. Lithos, 30, 167–189.

Rancourt, D.G., Christie, I.A.D., Royer, M., Kodama, H., Robert J.-L., Lalonde, A.E., and Murad, E. (1994) Determination of accurate $^{[4]}Fe^{3+}$, $^{[6]}Fe^{3+}$, and $^{[6]}Fe^{2+}$ site populations in synthetic annite by Mössbauer spectroscopy. American Mineralogist, 79, 51–62.

Reid, D.L., Welke, H.J., Erlank, A.J., and Betton, P.J. (1987) Composition, age and tectonic setting of amphibolites in the central Bushmanland Group, western Namaqua Province, South Africa. Precambrian Research, 36, 99–126.

Ryan, P.J., Lawrence, A.L., Lipson R.D., Moore, J.M., Paterson, A., Stedman, D.P., and Van Zyl, D. (1986) The Aggeneys base metal sulphide deposits, Namaqualand district. In C.R. Annhaeusser and S. Maske, Eds., Mineral deposits of Southern Africa, vol. II, p. 1447–1474. Geological Society of South Africa, Johannesburg, South Africa.

Solie, D.N., and Su, S.-C. (1987) An occurrence of Ba-rich micas from the Alaska Range. American Mineralogist, 72, 995–999.

Swope, R.J., Munoz, J.L., Smyth, J.R., and Zanetti, K.A. (1994) Crystal chemistry of 1*M* ferromagnesian micas: A single crystal X-ray study. Geological Society of America Abstracts with Programs, 26(7), A-166.

Tracy, R.J. (1991) Ba-rich micas from the Franklin Marble, Lime Crest and Sterling Hill, New Jersey. American Mineralogist, 76, 1683–1693.

Valley, J.W., Petersen, E.U., Essene, E.J., and Bowman, J.R. (1982) Fluorphlogopite and fluortremolite in Adirondack marbles and calculated C-O-H-F fluid compositions. American Mineralogist, 67, 545–557.

Waters, D.J. (1989) Metamorphic evidence for the heating and cooling path of Namaqualand granulites. In J.S. Daly, R.A. Cliff, and B.W.D. Yardley, Eds., Evolution of metamorphic belts. Special Publication of the Geological Society, 43, 357–363.

Willner, A. (1992) Tourmalinites from the stratiform peraluminous metamorphic suite of the central Namaqua Mobile Belt (South Africa). Mineralium Deposita, 27, 304–313.

Willner, A., Schreyer, W., and Moore, J.M. (1990) Peraluminous metamorphic rocks from the Namaqualand Metamorphic Complex (South Africa): Geochemical evidence for an exhalation-related, sedimentary origin in a Mid-Proterozoic rift system. Chemical Geology, 81, 221–240.

Yardley, B.W.D. (1985) Apatite compositions and the fugacities of HF and HCl in metamorphic fluids. Mineralogical Magazine, 49, 77–79.

Yoshii, M., and Maeda, K. (1975) Relations between barium content and the physical and optical properties in the manganoan phlogopite-kinoshitalite series. Mineralogical Journal, 8, 58–65.

Yoshii, M., Maeda, K., Kato, T., Watanabe, T., Yui, S., Kato, A., and Nagashima, K. (1973a) Kinoshitalite, a new mineral from the Noda-Tamagawa mine, Iwate Prefecture. Chigaku Kenkyu, 24, 181–190 (in Japanese).

Yoshii, M., Togashi, Y., and Maeda, K. (1973b) On the intensity changes of basal reflections with relation to barium content in manganoan phlogopite and kinoshitalite. Bulletin of the Geological Survey, Japan, 24, 543–550.

Zhu, C., and Sverjensky, D.A. (1991) Partitioning of F-Cl-OH between minerals and hydrothermal fluids. Geochimica et Cosmochimica Acta, 55, 1837–1858.

Manuscript received October 5, 1994
Manuscript accepted March 22, 1995